Molecular-scale noncontact atomic force microscopy contrasts in topography and energy dissipation on c(4x2) superlattice structures of alkanethiol self-assembled monolayers

AUTHOR(S):

Fukuma, Takeshi; Ichii, Takashi; Kobayashi, Kei; Yamada, Hirofumi; Matsushige, Kazumi

CITATION:

Fukuma, Takeshi ...[et al]. Molecular-scale noncontact atomic force microscopy contrasts in topography and energy dissipation on c(4x2) superlattice structures of alkanethiol self-assembled monolayers. JOURNAL OF APPLIED PHYSICS 2004, 95(3): 1222-1226

ISSUE DATE:

2004-02-01

URL:

http://hdl.handle.net/2433/39707

JOURNAL OF APPLIED PHYSICS VOLUME 95, NUMBER 3 1 FEBRUARY 2004

Electron emission properties of Spindt-type platinum field emission cathodes

Y. Gotoh,[a] M. Nagao,[b] D. Nozaki, and K. Utsumi
Department of Electronic Science and Engineering, Kyoto University, Yoshida-honmachi, Sakyo-ku, Kyoto 606-8501, Japan

K. Inoue, T. Nakatani, T. Sakashita, and K. Betsui
Fujitsu Laboratories, Inc., 64, Nishiwaki, Okubo-cho, Akashi 674-8555, Japan

H. Tsuji and J. Ishikawa
Department of Electronic Science and Engineering, Kyoto University, Yoshida-honmachi, Sakyo-ku, Kyoto 606-8501, Japan

(Received 3 December 2002; accepted 28 October 2003)

Electron emission properties of Spindt-type platinum field emission cathodes were investigated. The current–voltage characteristics together with the current fluctuation during long term operation were evaluated in ultrahigh vacuum. The changes of the emission properties in hydrogen, oxygen or carbon monoxide gas ambient were also investigated. Significant improvement of the emission properties was found when the cathode was operated in carbon monoxide ambient under a certain condition. It was found that the effect of the improvement lasted at least 200 h, and resistance against the oxygen exposure was also improved. The changes of the electron emission properties during long term operation in ultrahigh vacuum and in gas ambient were analyzed with the Seppen–Katamuki chart, of which ordinate and abscissa are slope and intercept of Fowler–Nordheim plot. The electron emission properties were distributed along a straight line in the Seppen–Katamuki chart, and those of the cathode improved by carbon monoxide exposure were distributed along another line. The deviation of the electron emission property in ultrahigh vacuum was considered to be due to change in the geometry of the emitting surface. The major reason for the modification of electron emission properties in carbon monoxide ambient was considered to be deposition of carbon onto the emitting surface, resulting in reduction of the work function. From the deviation of the Fowler–Nordheim characteristics in the Seppen–Katamuki chart, we presented an empirical equation for field emission. © *2004 American Institute of Physics.* [DOI: 10.1063/1.1635655]

I. INTRODUCTION

Recently, development of flat-panel displays (FPDs) has been performed with liquid crystal displays, plasma display panels and organic electroluminescent devices as well as field emission displays (FEDs).[1] Among these displays, the FED[2,3] is one of the promising candidates for the future display, because of higher brightness, wider view angle, and high resistance against the operating circumstances. Although there are some cathodes such as thin-film type and carbon nanotubes, a Spindt-type cathode[4,5] still locates at a closer position to the FPD as a commercial product. One of the difficulties in realizing FED is such that the field emission device is generally unstable, particularly in poor vacuum conditions, and therefore stability and life are not satisfactory. This is a serious problem for the FED, because the FED has a large surface to volume ratio, and thus even a small amount of gas desorption from the device may cause pressure increase. Together with this, reduction in an operating voltage is also one of the important issues for the FED, from the circuitry requirements. Owing to the above background, development of the Spindt-type cathode which can be operated in a relatively poor vacuum at a low voltage is one of the most important subjects. Since the current fluctuation is mainly due to the adsorption and desorption of the residual gas molecules onto the emission site,[6–9] the stability of the cathode is dependent primarily on the reactivity of the emitting surface. Consequently, it is easily supposed that selection of the cathode material is important. However, not so much research on the selection of the cathode material has been reported so far.[10–13] In the above-mentioned research, materials with low work function, for example, titanium (Ti) were overcoated on a molybdenum (Mo) emitter[11,13] or the emitter itself was made of transition metal.[10] There are only a few reports that concern the cathode with a noble metal emitter.[12]

As for the operation in gas ambient, some reports can be seen in the literature.[14–21] According to these reports, it was shown that methane (CH_4) improved the emission property[15,19] but carbon dioxide CO_2 was poisonous.[18] If we have some information about the effectiveness of environmental gas, we can suppress or add some gas molecules in the vacuum tube, according to its effect on the cathode. However, results seen in the literature are mostly concerned

[a]Author to whom correspondence should be addressed; electronic mail: ygotoh@kuee.kyoto-u.ac.jp
[b]Present address: National Institute of Advanced Industrial Science and Technology, AIST 2, Umezono 1-1-1, Tsukuba, Ibaraki 305-8568, Japan.

with the Mo emitters, and not for the other materials.

We have investigated the electron emission properties of the Spindt-type cathodes made of various emitter materials, and found that platinum (Pt) exhibited a superior property to the other materials of nickel (Ni), molybdenum (Mo) and gold (Au).[12] In this article, we report the electron emission properties of the Spindt-type Pt field emission cathodes in detail. We measured long term stability of the current–voltage ($I-V$) characteristics and investigated the changes in the emission pattern. We also examined the resistance against hydrogen (H_2), oxygen (O_2), and carbon monoxide (CO) gas exposure. Among the gases investigated, CO improved the emission property significantly[22] and also the resistance against O_2 was improved.[23] We summarize these results here in this article.

We not only summarize the experimental results, but also examine the Fowler–Nordheim (FN) characteristics of the Pt field emission cathodes in detail. It is generally impossible to extract the physical parameters of the emitting surface from the FN plot, because of the difficulties in determining the physical parameters of apex radius r, emission area α, and work function ϕ. Estimation of ϕ has long been performed with the slope of the FN plot.[24,25] It has been difficult to argue the intercept, particularly for the materials that are greatly affected by gas adsorption. We arranged FN plots of the Pt cathodes in the Seppen–Katamuki (SK) chart,[26] and found a clear relationship between the intercept and slope of the FN plots. From the obtained relationship, we derived an empirical relationship among the physical parameters and give a grid of the equi-work function and equi-apex radius.

II. FABRICATION OF PLATINUM CATHODES

The Spindt-type Pt cathodes were fabricated by our process,[27] which followed that of Spindt *et al.*[4] The optimum configuration of the electrodes was already examined, and it is known that the best emission property can be obtained with the emitter of which apex comes to the upper surface of the gate electrode.[10,28] However, it is also well known that the shape of the emitter is strongly dependent on the material; apex cone half angle depends upon the material.[10,27] In the fabrication process of the Spindt cathodes, the radius of the base face of the emitter is uniquely determined by the diameter of the gate hole. Consequently, the height of the cone differs among the emitter material. So, it is generally troublesome to satisfy the above condition for a given emitter material with a predetermined microfabrication process. For example, Pt formed a thinner cone as compared to Mo, and thus the emitter height exceeds the gate electrode, resulting in the formation of a protruding emitter. In the present study, we adjusted the emitter height by inserting materials which have lower aspect ratios.[12] No resistive layer was inserted in order to investigate the essential property of electron emission from the Pt cathode. Here in this article, we describe the results for one-tip cathodes, although we measured the properties also for the arrayed cathodes.[21] Figure 1

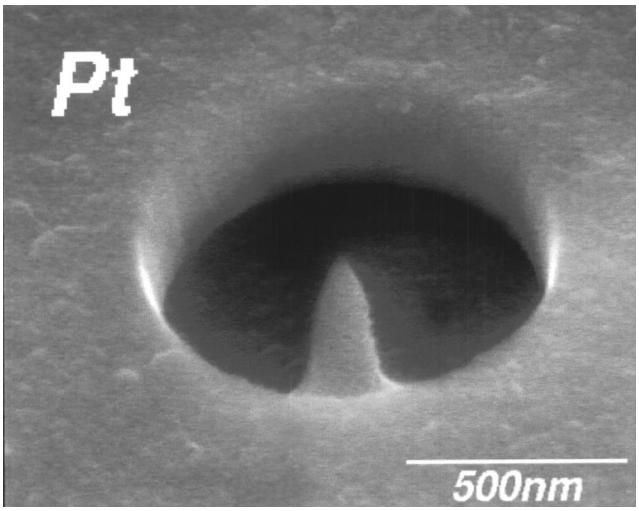

FIG. 1. Scanning electron micrograph of the fabricated Pt emitter.

shows a scanning electron micrograph of the fabricated Pt cathode. The gate aperture was approximately 1 μm. The apex radius seems to be less than 20 nm.

III. EXPERIMENTAL PROCEDURES

A. System for measurement of electron emission properties

The measurements of the electron emission properties were performed in an ultrahigh vacuum chamber. We first evacuated the chamber with a turbo-molecular pump, and baked the chamber. After the baking was over, we switched the pumping system from the turbo-molecular pump to a sputter ion pump and a Ti sublimation pump. The background pressure was $1-2\times10^{-7}$ Pa. Figure 2 shows a schematic diagram of the measurement system. The sample was settled on a TO-5-type mount. The gate electrode was grounded and a negative bias (V_{EG}) was applied to the emitter. A collector was settled at approximately 5 mm apart from the cathode. The collector was a silicon substrate or the phosphor coated conductive glass plate, and we applied a

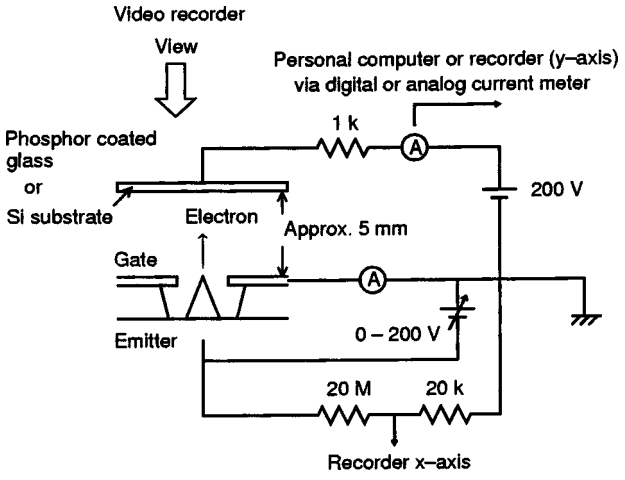

FIG. 2. Schematic drawing of the measurement system.

fixed positive bias of 200 V to it. The collector current I_C was measured by a digital ammeter at floating potential.

$I_C - V_{EG}$ characteristics were recorded in a digital computer through the ammeter via general purpose interface bus. Current fluctuation was also recorded to the digital computer. Sampling time of this recording system was approximately 0.25 s. Emission patterns projected on a phosphor screen were recorded by a video camera through a view port. Gas introduction was carefully made through a variable leak valve. The purity of the gas was confirmed by a quadrupole mass analyzer.

B. Aging process

Prior to the measurement, we heated the cathode up to 150 °C for 1 h, in order to eliminate the adsorbed moisture molecules. The cathode was then operated in the ultrahigh vacuum for several hours. During this process we gradually increased V_{EG} until I_C reached 20 μA, which we call *aging*. With this aging, we can remove some unstable sharp protrusions on the emitting surface, resulting in more stable operation. The aging was terminated when the current fluctuation became sufficiently small: when the normalized noise power, of which definition will be described later, reached 10^{-3}.

C. Procedure of measurements

The investigations that will be described in the following are categorized into three different schemes. The first is a long term measurement of the emission property in ultrahigh vacuum (UHV). The second is a measurement in H_2 and O_2 ambient. The last is the improvement of emission property by operating the cathode in CO ambient. Detailed procedure of each measurement will be described later, in the corresponding section.

D. Analysis of electron emission property

The stability of the emission current was evaluated by calculating the normalized noise power of the current fluctuation. The detailed procedure of the calculation is shown elsewhere.[26] The current fluctuation in the duration of 75 s, which was recorded in the PC, was converted to a power spectral density (PSD) function through Fourier transform. The noise power was calculated by integrating the PSD between 0.2 and 2 Hz. The noise power was normalized by the direct current component. Since the current fluctuation of the field emitter has a frequency dependence of approximately f^{γ}, $1<\gamma<2$,[6–9] the low frequency component well represents the stability.

Here in this study, the Seppen–Katamuki analysis[26] was used to understand the emission property of the cathodes. We have investigated the electron emission from many kinds of deposited materials including metals,[26,29] transition metal nitrides,[30–32] and diamonds with different surface states,[33] and found that there is an empirical relation between the slope and intercept of the Fowler–Nordheim (FN) plot.[29,32,33] So far, intercept and slope were used to express the FN characteristics, for example, as *Fowler–Nordheim's a and b*,[5] no one made a two-dimensional diagram. Plotting the FN characteristics on a two-dimensional diagram of which abscissa and ordinate are the intercept and the slope of the FN plot, respectively, we can understand the relative changes of the work function and emission area/apex radius. We call this two-dimensional diagram ''Seppen–Katamuki Chart'' or ''SK Chart,'' seppen and katamuki are the Japanese words that correspond to the intercept and slope, respectively. It should be noted that this empirical relation between intercept and slope does NOT agree with the theoretical prediction which is based on the calculation assuming a smooth surface.[34] This is because the emitting surface is not atomically smooth. What we call the SK chart is, therefore, not a simple diagram of the slope and intercept that can be understood by the conventional modeling of field emission. Figure 3 shows typical examples of the FN characteristics in the SK chart. In this figure, one plot correspond to a FN characteristic of one nickel deposited tungsten emitter. The upper right side and lower left side show the lower and higher work functions, respectively. The upper left side and lower right side show the smaller and larger emission areas/apex radii. This method is useful for the comparison between different cathodes, and changes in gas introduction.[35]

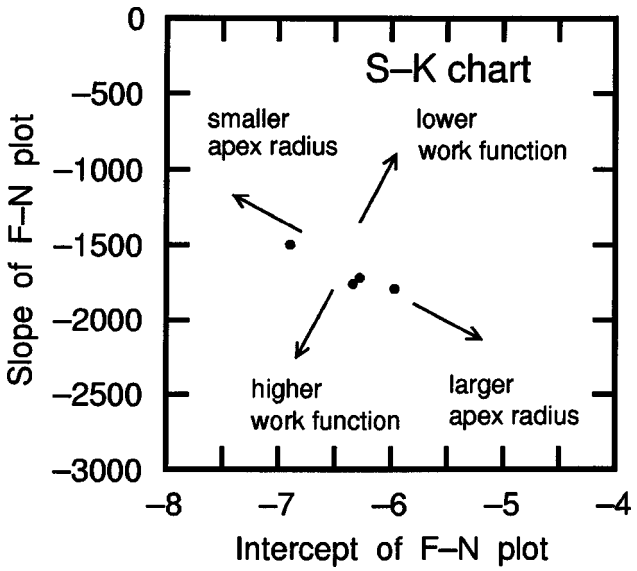

FIG. 3. Example of the SK chart. Interpretation of FN characteristics in this chart is also illustrated in the figure.

IV. EXPERIMENTAL RESULTS

A. Emission properties in ultrahigh vacuum

1. Current–voltage characteristics

Figure 4 shows a typical example of FN plot for $I_C - V_{EG}$ characteristics of the Spindt-type Pt cathode. In this figure, the electron emission properties of the Spindt-type cathodes made of different materials are also illustrated.[12] The Pt cathode provided a higher current at a lower voltage, as compared to the cathodes with other materials.

2. Change in emission current

The Pt cathodes were tested for a long term stability. After the aging process, we applied V_{EG} so that the cathode could emit I_C of 1 μA at the initial stage. The emitter was

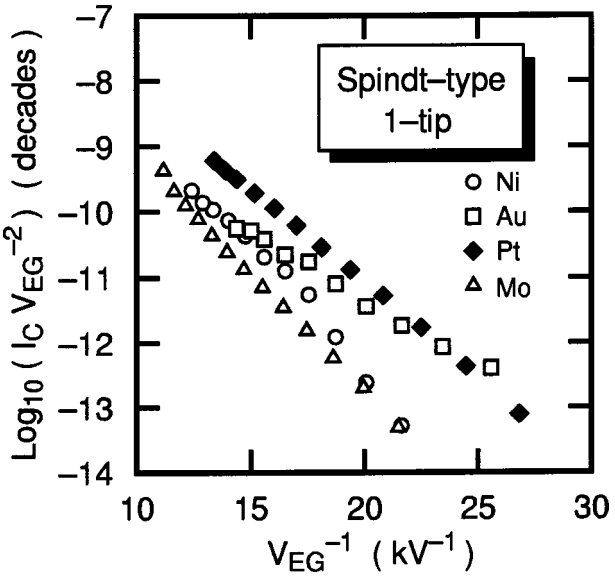

FIG. 4. Typical example of $I_C - V_{EG}$ characteristics for the Spindt-type Pt cathode together with those for the Spindt-type cathodes made of other material.

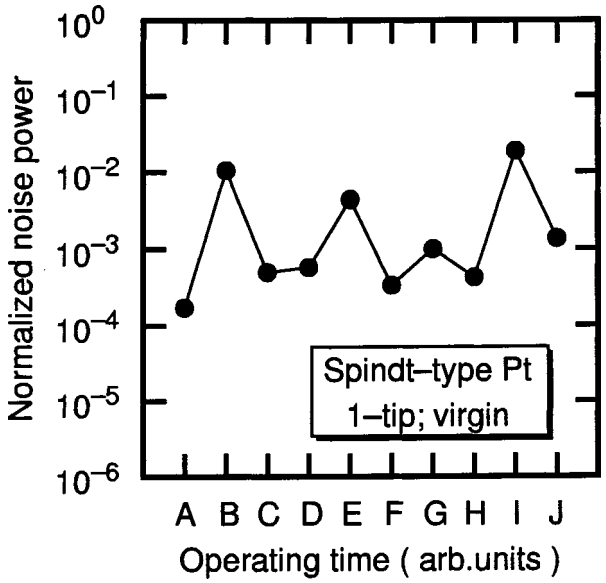

FIG. 6. Short term stability of the current of the Pt cathode during the long term stability measurement in UHV.

then operated in UHV for about 150 h. The change in I_C was recorded in a digital computer with an appropriate interval. Sometimes, typically every 24 h, the emission was interrupted, and $I_C - V_{EG}$ characteristics and current fluctuation were acquired. Also the emission pattern was recorded in a video camera at the same time.

The change in the emission current during the course of the measurement is shown in Fig. 5. The FN characteristics are labeled in alphabetical order in accordance with the order of the measurements. It should be noted that V_{EG} was adjusted within several volts to obtain 1 μA emission after each $I_C - V_{EG}$ measurement, and thus V_{EG} was not the same throughout the test. Although the current deviation is relatively large, no significant degradation of the emission property throughout the measurement was seen.

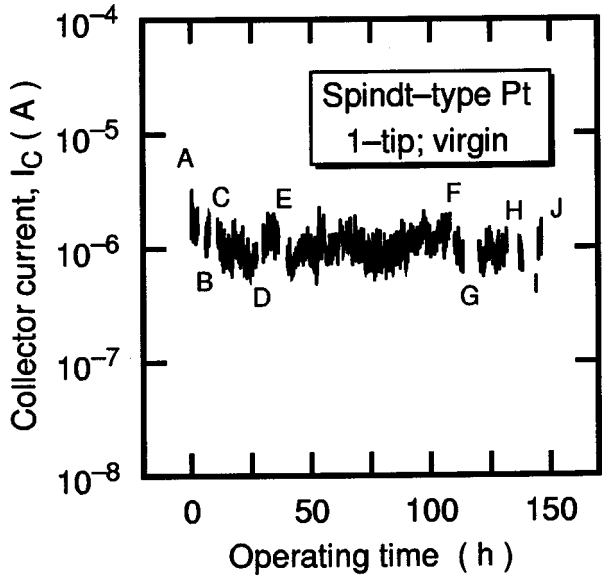

FIG. 5. Deviation of the current of the single tip Pt cathode during the long term stability measurement in UHV.

Figure 6 shows the short term current stability of the Pt cathode. The normalized noise power was almost 10^{-4} and occasionally it increased up to 10^{-2}. These noisy characteristics were obtained at B, E, and I, labeled in Fig. 5 and we will discuss the relationship between the stability and $I_C - V_{EG}$ characteristics in the following.

3. Change in current–voltage characteristics

The emission current deviation in FN plot is shown in Figs. 7(a) and 7(b), which are the changes in FN plot and those of the FN characteristics in the SK chart, respectively. In Fig. 7(a), four typical $I_C - V_{EG}$ curves are illustrated by thick solid, broken, dot-dashed, and dashed lines. Although the $I_C - V_{EG}$ curves are not completely straight, particularly at the higher current, we can fit the characteristics to straight lines at the medium current range. The fitted lines are indicated by thin solid lines. From the figure, it is shown that the slope changes when the current changed. It is interesting to see that the fitted lines go through a single point. We will discuss this later. From Fig. 7(b), it is noted that the FN plots are distributed along a straight line. Such a distribution is already obtained by us, as shown in Fig. 3, and also by Watanabe *et al.* with carbon related materials[36] and Mackie, Xie, and Davis with transition metal carbides.[37] However, we do not see any order of changes of the slope; the slope sometimes became smaller and sometimes larger. At the points B, E and I, where the emission current fluctuation was large, the FN characteristics are located at the lower right side.

4. Emission pattern

Figures 8(a)–8(d) show the emission patterns of the Pt cathode at different $I_C - V_{EG}$ characteristics. The patterns shown in Figs. 8(a)–8(d) correspond to the points H, A, E, and B, respectively. These positions are arranged in this or-

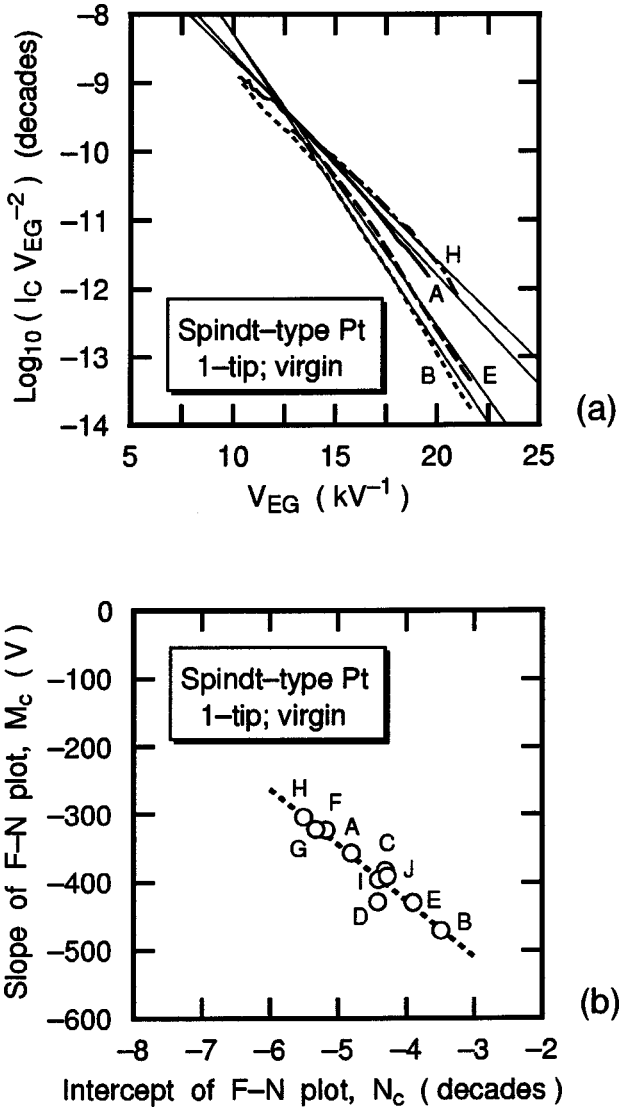

FIG. 7. Change of emission property during the long term measurement. (a) Changes in FN plot, and (b) changes of FN plot in the SK chart.

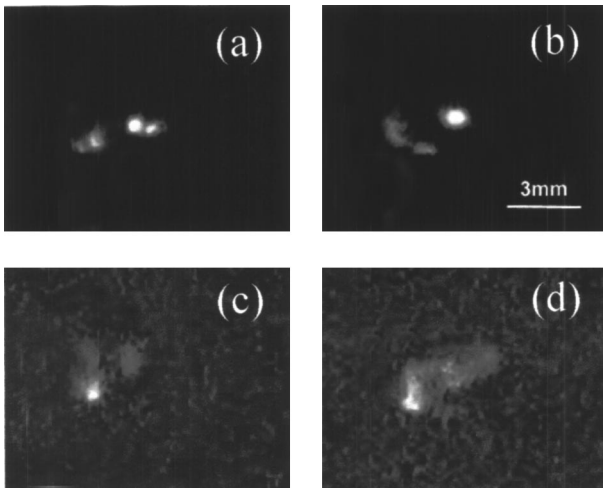

FIG. 8. Changes in emission pattern at different $I_C - V_{EG}$ characteristics. The images correspond to the points of (a) H, (b) A, (c) E, and (d) B.

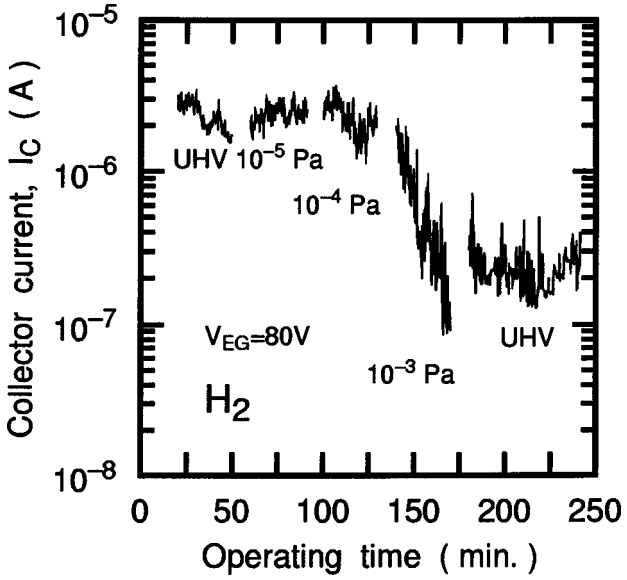

FIG. 9. Changes of I_C in H_2 ambient.

der in the SK chart from upper left to lower right. From the figure, the emission patterns at H and A are spot-like but those in E and B spread to wide area. The spot pattern would be attributed to the microstructure on the emitting surface, such as an atomic protrusion. According to the interpretation of the SK chart, the emission area is smaller for H, A, E, and B, in this order. The emission pattern agreed well with our interpretation. It was experimentally shown that the cathode of which FN characteristic locates at upper left side shows a smaller emission area.

B. Emission properties in gaseous ambient

1. Introduction of gas

Either H_2 or O_2 gas was introduced to the vacuum chamber, while the cathode was being operated. For both cases, gas was first introduced to 10^{-5} Pa, and the current fluctuation was measured for approximately 30 min. After that, the chamber was evacuated once and we measured the $I_C - V_{EG}$ characteristics and current fluctuation. Then, we introduced the gas again, but to higher pressure. This sequence was repeated at the gas pressures of 10^{-4} and 10^{-3} Pa. Finally, the chamber was evacuated and the emission property in UHV was again measured.

2. Hydrogen ambient

Figure 9 shows the change in I_C due to H_2 gas introduction. I_C of the Pt cathode did not change significantly up to 10^{-4} Pa, but it gradually decreased when H_2 gas was introduced to 10^{-3} Pa. Although improvement of the electron emission property in H_2 ambient were reported for Mo cathode,[14] the Pt cathodes did not show any improvement under H_2 gas ambient. The results for Ni and Au cathodes were similar to the results for the Pt cathodes.[38]

3. Oxygen ambient

The change of I_C of the Pt cathode in O_2 gas ambient is shown in Fig. 10. I_C rapidly decreased at the very initial

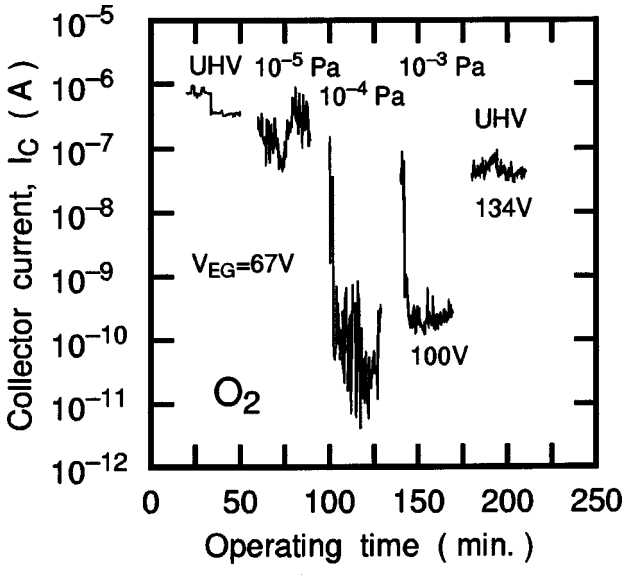

FIG. 10. Changes of I_C in O_2 ambient.

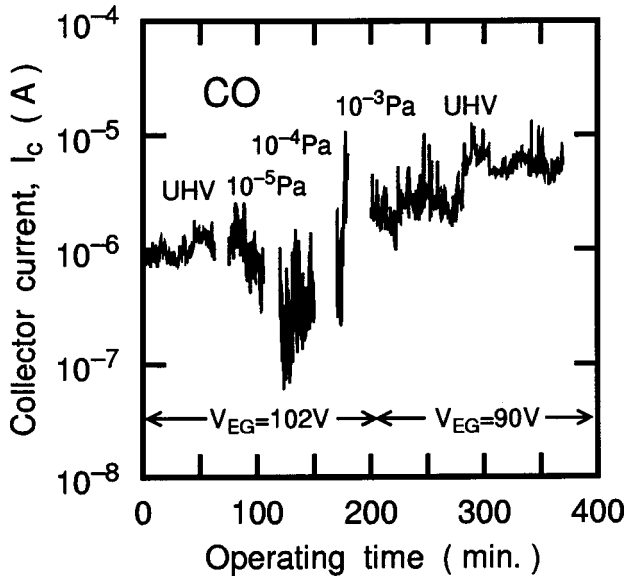

FIG. 11. Changes of I_C in CO ambient.

stage of 10^{-4} Pa gas introduction, and after several minutes I_C became almost constant. This phenomenon would be closely related to the adsorption of oxygen molecules onto the emitting surface. Generally, adsorption of oxygen gas results in the higher work function. I_C again rapidly decreased at 10^{-3} Pa gas introduction. The repeated occurring of rapid decrease in 10^{-3} Pa may be associated with the fact that we evacuated the oxygen gas once, after 10^{-4} Pa introduction, as described in the experimental procedure. This together with the I_C-V_{EG} measurement in UHV might result in desorption of some of the oxygen molecules from the emitting surface. As written in the figure, V_{EG} became higher as the O_2 gas was introduced. The noise power measured at I_C of 40 nA increased in proportion to the O_2 gas pressure.[21]

Even for the Pt cathode, the electron emission property was affected by O_2 gas ambient. However, in comparison to the other materials such as Mo and Ni,[21] the Pt cathode was more durable against the exposure to O_2 gas ambient.

C. Change in emission properties in carbon monoxide ambient

1. Exposure to carbon monoxide ambient

Experiments for the investigation of the change in emission characteristics due to exposure to CO ambient were performed in a similar way that is described above. Figure 11 shows the change in emission current during operation in CO gas ambient. We set the initial emission current I_C to 1 μA. Operation in 10^{-5} Pa did not show any significant change, but I_C gradually decreased. At 10^{-4} Pa, I_C further decreased. However, in 10^{-3} Pa, I_C rapidly increased. The operation was interrupted when the rapid increase was observed, and the introduced CO gas was evacuated. At this time, I_C increased to be several microamps at 90 V. If we did not interrupt the operation, the cathode was destroyed due to excess current. Taking the fact into consideration that the improvement of the Mo cathode by CH_4 gas introduction is about 10% increase of the emission current,[10] the present improvement is highly effective. The above improvement was seen for several cathodes, but for all the cases, it was necessary that the initial current is approximately 1 μA, irrespective of V_{EG}. If we set the current differently, for example, 5 or 10μA, significant improvement was not observed. Although the mechanism of this improvement has not been clarified as yet, the presence of carbon atoms or layers on the surface of the emitter would be attributed to the improvement. These carbon atoms or layers may be formed by electron beam enchanced deposition of carbon atoms, or by catalytic reaction on the emitter surface. These carbon atoms may be removed by ion bombardment or temperature increase of the emitter. Formation of such a layer is dependent on the deposition and desorption of carbon atoms, which are determined by the rate of the above reactions, sputtering, and temperature increase. All these rates are related to the emission current. The presence of the emission current appropriate for the improvement can be understood if these rates are related to each other, although the detailed procedure could not be drawn. Hereafter, we call this procedure for improvement of emission properties the CO treatment.

We also tried to improve the emission properties of the Spindt-type Ni cathodes, and only a slight change in the emission current was observed.

2. Current–voltage characteristics

Figure 12 shows the I_C-V_{EG} characteristics of the Pt cathode before and after the CO treatment. The characteristics are shown in a FN plot. This treatment could apply at least twice. Figure 13 shows the FN characteristics of the virgin cathode, after the first treatment, and after the second treatment plotted in the SK chart. As is the same with the UHV case shown in Fig. 7(b), the FN characteristics are arranged along a line. The slopes of these lines are −82.4, −62.6, and −49.8 V, respectively. As the position shifts to the upper right, the line had more gentle slope. It should be noted that these lines also go through a common point. We will discuss the results further in Sec. V.

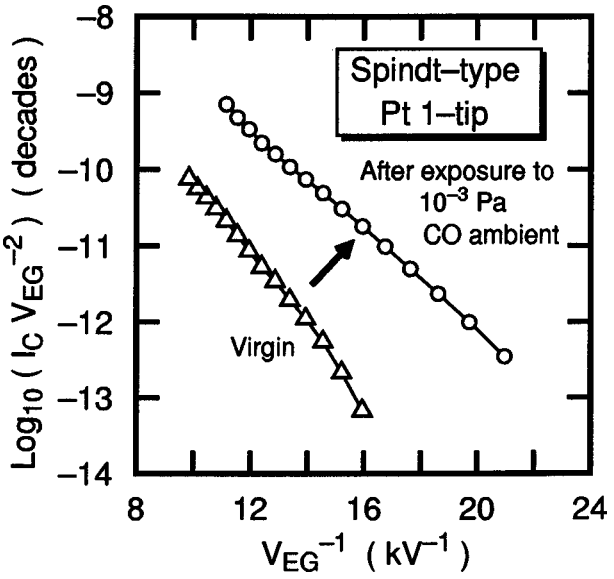

FIG. 12. Changes of FN characteristics before and after CO treatment.

3. Short term stability

Figures 14(a) and 14(b) show the typical examples of the current fluctuation before and after the CO treatment. Flicker noise was largely reduced by the present process. The calculated noise powers were 1.4×10^{-5} before CO treatment and 1.6×10^{-6} after the CO treatment.

4. Life test

Life test was performed to confirm that the improved characteristics are maintained for a long time. Figure 15 shows the current variation in a long time range. The cathode was operated at 51 V in UHV. Although I_C varied from 0.01 to 0.2 μA, the cathode could be operated for more than 400 h. Since the virgin cathode yielded less than 0.1 nA at 51 V, the effect of improvement was not lost during the operation.

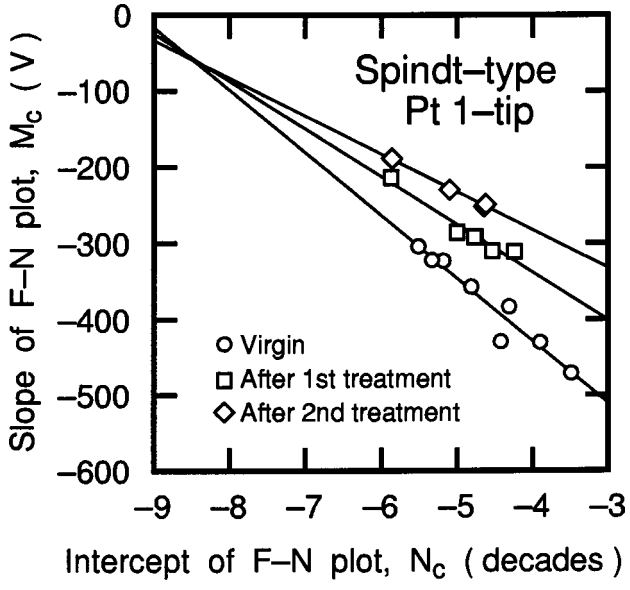

FIG. 13. Changes of electron emission property before and after CO treatment.

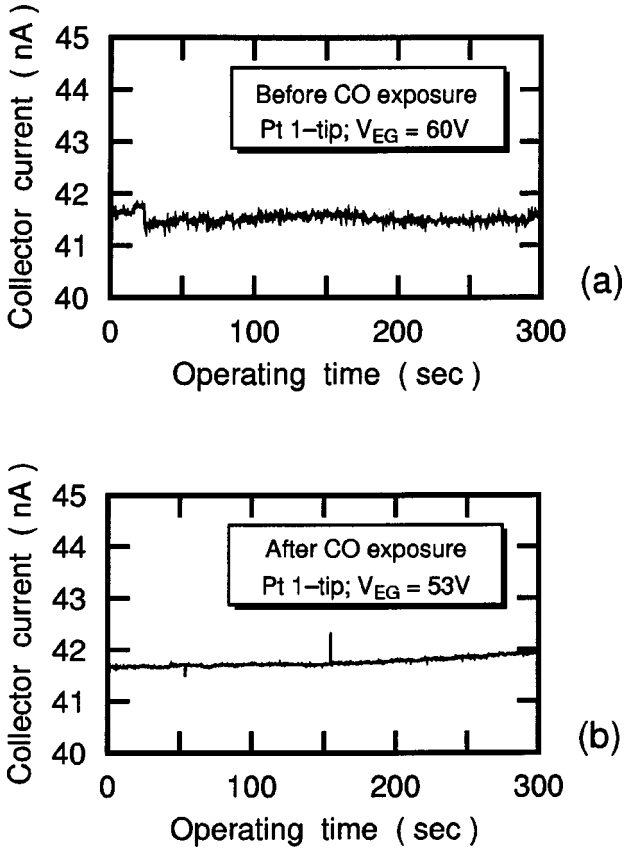

FIG. 14. Changes in short time current fluctuation (a) before and (b) after CO treatment.

During the measurement of the above characteristics, $I_C - V_{EG}$ characteristics were measured every 24 h interval. The time the $I_C - V_{EG}$ curve was measured is indicated in Fig. 15 by letters $a-k$.

Current fluctuation and driving voltage were measured at these points and the results are shown in Fig. 16. Here the driving voltage is defined as the voltage required to extract

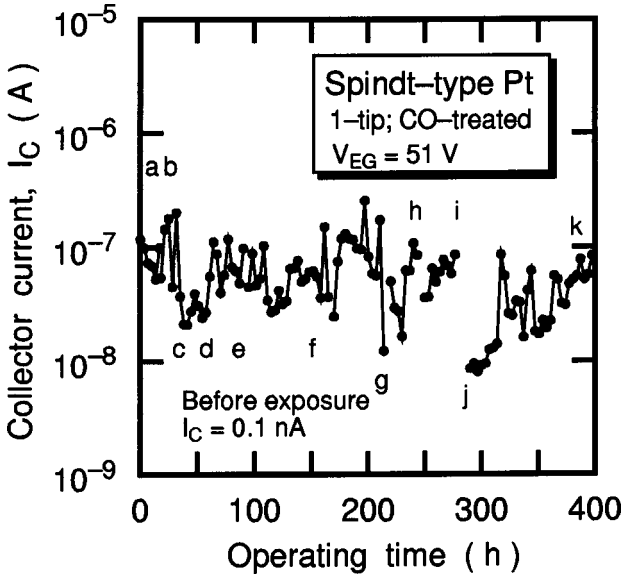

FIG. 15. Life test for the improved cathode.

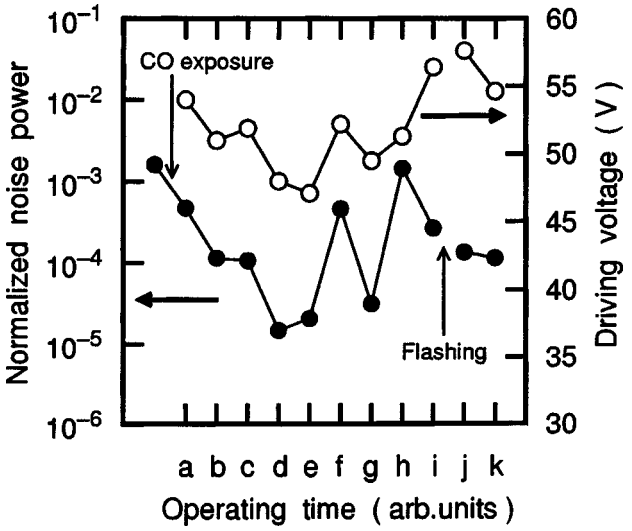

FIG. 16. Changes in current fluctuation and operating voltage during life test for the CO-treated cathode.

40 nA. The current fluctuation first decreased but tended to increase at the point *d*, when the operation continued for 50 h. After the point *d*, driving voltage also increased. At the point *i*, we performed a flashing, and the current fluctuation decreased, although I_C at the same voltage decreased. After this flashing, the current gradually recovered, and finally at the point *k*, I_C reached the initial value just after the CO treatment.

Considering that the improvement of the emission property by H_2 introduction was rapidly degraded,[14] the present improvement is long lasting and effective.

5. Emission pattern

The virgin Pt cathodes showed alternative emission from multiple sites during operation in UHV. After the CO treatment, the emission pattern was fixed and did not change significantly.

6. Resistance against oxygen

The changes in electron emission characteristics when the cathode is subjected to O_2 gas ambient were compared between the virgin and CO-treated cathodes. I_C first decreased rapidly and then the rate of decrease became smaller for both cathodes. The final current in O_2 ambient was about two orders of magnitude lower than that in UHV. After exposure to 10^{-3} Pa, the O_2 gas was evacuated and the emission characteristics of the emitter were examined in an UHV environment.

Figures 17(a) and 17(b) show the changes of the emission characteristics in the SK chart through the operation in O_2 ambient for the virgin and CO-treated cathodes, respectively. For the virgin cathode, the shift due to O_2 exposure is larger, whereas the shift is smaller for the CO-treated cathode. From these results, the resistance against O_2 introduction was improved through the CO treatment. This figure also shows the emission characteristics a long time after the evacuation of O_2 gas. The final characteristics in Figs. 17(a) and 17(b) are those after 3 and 14 h, respectively. From these

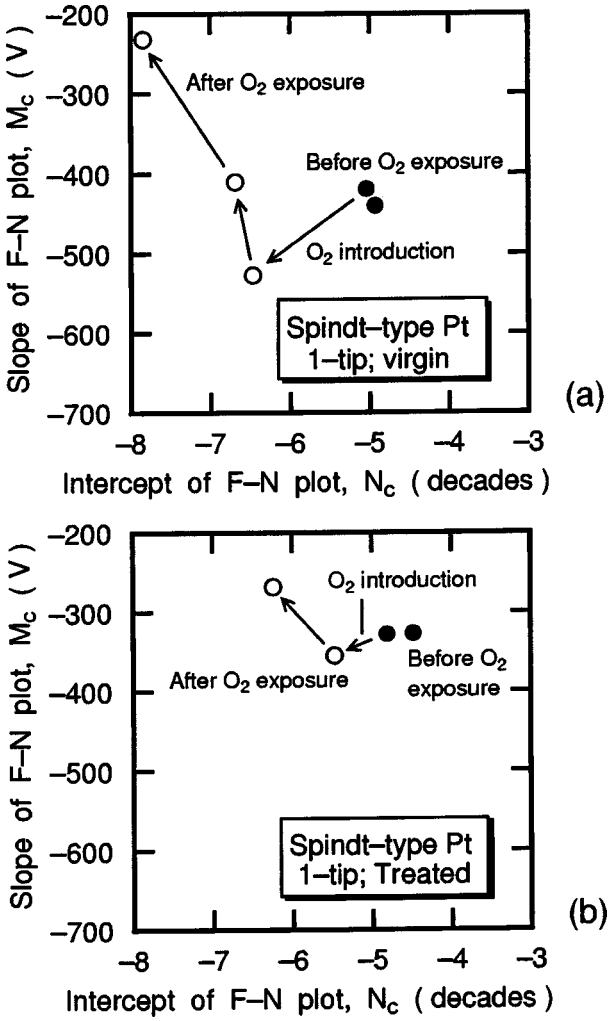

FIG. 17. Endurance against oxygen exposure after CO treatment.

results, it seems that the emission characteristics gradually recovered for both cathodes, but have a smaller emission area.

V. DISCUSSION

A. Equi-work function line

As described earlier, we consider that the linear distribution of the FN characteristics in the SK chart is due to the change in the apex radius r or in the emission area α rather than the change in the work function ϕ. The relation between ϕ and the location of FN characteristics in the SK chart has been confirmed experimentally with the field emission cathodes made of transition metal nitride thin films of which ϕ was controlled by controlling nitrogen composition.[32,39]

However, as for the relation between α or r and the location of FN characteristics in the SK chart, it has not been experimentally confirmed as yet, although we supposed that the upper left is smaller α or r and that the lower right is larger α or r. The present results in Figs. 7 and 8 gave an experimental evidence for this interpretation. The surface structure of a Pt emitter may change, possibly due to the surface migration of the Pt atoms, but maintain the clean surface. So, the lines shown in Fig. 13 are considered to be

equi-work function lines, and here, in the following argument, we assume that a set of FN characteristics located along one line in the SK chart has the same ϕ.

In the following, we will discuss the emission area, which is closely related to the apex radius r. Possibly we have some different structures on the emitting surface: sometimes fairly dull surface, and sometimes small protrusions on the base surface. However, the presence of multiple small protrusions is not likely in this case, because the observed emission patterns consisted of one major area, as shown in Figs. 8(a)–8(d). Also, we confirmed that the protrusion present on the emitting surface, if any, would not be so small to have a special effect on the field emission such as nanotips. It is known that a nanotip sometimes shows different behavior as compared to the conventional emitter. One remarkable difference would be the energy distribution of emitted electrons measured by Binh and Purcell.[40] They observed multiple peaks in the energy distribution for nanotips. We have made the energy distribution measurement of the Pt cathode and found that there was no evidence for nanotip, showing typical energy distribution from the metallic emitter.[41]

It should be noted that the following discussion is for very rough modeling of the field emission, especially about the fact as to why the emission properties are arranged in a line in the SK chart. So, here we define apparent apex radius "r." This may be larger than the actual apex radius of the protrusion on the surface, and may be smaller than the apex radius of the base emitter. A detailed argument with precise calculations like those made by Mackie, Xie, and Davis[37] will be a future subject.

B. Linear distribution of FN characteristics in SK chart

The relation between the field emitted current I (in this case I_C) and the applied voltage V (in this case V_{EG}) can be expressed using the FN equation with image force correction[42]

$$I=\alpha J=\frac{a\alpha}{t^2(y)}\frac{\beta^2V^2}{\phi}\exp\left[-\frac{b\phi^{3/2}}{\beta V}v(y)\right], \tag{1}$$

where α is the effective emission area and β is the voltage-to-local field conversion factor; ϕ is the work function; $a=e^3/8\pi h$, and $b=8\pi\sqrt{2m}/3he$ where e is the elementary charge; π is the circular constant; h is the Planck constant, and m is the electron mass; y is the lowering of the surface potential barrier due to the combination of image force and high field; $t(y)$ and $v(y)$ are the resulting correction factors. Although a modified formulation for field emission current density has been proposed,[43,44] here we use the conventional equation. The slope (M_n) and intercept (N_n) of a FN plot drawn with the abscissa and ordinate of $1/V$ and natural logarithm of I/V^2 will be

$$M_n=-\frac{0.95b\phi^{3/2}}{\beta},\qquad N_n=\ln\left(\frac{a\alpha\beta^2}{1.1\phi}\right)+\frac{N_n'}{\phi^{1/2}}. \tag{2}$$

Here we simplified the equation with the approximation of $t^2(y)=1.1$ and $v(y)=0.95-y^2$.[4] $N_n'=\sqrt{8m}e^2/3h\epsilon_0$ contains no variables α or β. The subscript n means that these values are calculated with the ordinate that was scaled in natural logarithm. It should be noted that in the intercept and slope with the common logarithm, the above values should be replaced by $M_c=M_n/\ln 10$ and $N_c=N_n/\ln 10$, respectively. Figure 13 is plotted with the abscissa of $1000/V$, but the calculation of the slope here will be made with respect to $1/V$. As for the ordinate, common logarithm ($\log_{10} I/V^2$) will be used. With these parameters, any individual FN plot can be written in the form

$$\log_{10} I/V^2=\frac{\ln I/V^2}{\ln 10}=N_c+M_c\frac{1}{V}. \tag{3}$$

Since we observed a linear relation between slope and intercept in the SK chart, we may write

$$M_c=AN_c+B_c, \tag{4}$$

where A and B_c are parameters for fitting the relation. Note that A is common for both cases of natural and common logarithms. Using Eq. (4) to substitute for N_c in Eq. (3) gives

$$\log_{10}(I/V^2)=-\frac{B_c}{A}+M_c\left(\frac{1}{V}+\frac{1}{A}\right). \tag{5}$$

So whatever the value of M_c, when $V=-A$ then $\log_{10}(I/V^2)=-(B_c/A)$. This means that all the FN plots associated with a straight line in the SK chart go through this common point.

It also follows from Eq. (4) that variations in N_c and M_c are related by

$$\delta N_c=A^{-1}\delta M_c. \tag{6}$$

This relation is also valid for N_n and M_n. We already assumed that each line in Fig. 13 corresponds to the emitter of which surface has the same ϕ, but differs in the values of α and β. With this assumption, we obtain

$$\left(\frac{\delta\alpha}{\alpha}+2\frac{\delta\beta}{\beta}\right)=\frac{0.95b\phi^{3/2}}{A\beta}\frac{\delta\beta}{\beta}. \tag{7}$$

Taking the fact into consideration that the voltage-to-local field conversion factor β is almost inversely proportional to the apex radius r, so $\delta\beta/\beta=-\delta r/r$, the equation above is modified to

$$\frac{\delta\alpha}{\alpha}=(2+C)\frac{\delta r}{r}, \tag{8}$$

$$C=-\frac{0.95b\phi^{3/2}}{A\beta}. \tag{9}$$

Note that the slope A is generally negative as shown in Fig. 13, and thus C is positive. If C is small, α is to be proportional to r^2. For the theoretically calculated distribution of FN plots, the slope A is very large (Fig. 3 of Ref. 34 or Fig. 1 of Ref. 45). It means that α is almost proportional to r^2. In the previous article,[46] we treated C as a constant, and obtained the relation $\alpha\propto r^{11}$, but actually C contains β, thus further detailed argument is necessary.

TABLE I. Slope and intercept of the line in the SK chart and estimated work function.

Parameters Units	B_c V	$B_c \ln 10$ V	A V	$-1/A$ V^{-1}	Estimated ϕ eV
Virgin	−757	−1740	−82.4	0.012	5.32 (assumed)
After 1st CO treatment	−589	−1360	−62.6	0.016	4.39
After 2nd CO treatment	−482	−1110	−49.8	0.020	3.77

With the approximation that is commonly used for the etched needle emitter, the following relation holds:[24]

$$\beta = \frac{1}{kr}. \tag{10}$$

Here it should be noted that k is determined by the macroscopic field distribution which is generally related to the electrode spacing d and also r, but weakly dependent on these physical parameters. Equation (10) is thus

$$\beta = \frac{1}{k} \times \frac{1}{r} = \beta_{\text{macroscopic}} \times \beta_{\text{microscopic}}. \tag{11}$$

For the isolated needle-type emitter, $k \sim 5$.[24] For the Spindt type, k is not known. However, considering that $r = 20$ nm and emission is seen at about 50 V for the present case, it is possible to assume k of 1∼2. The relationship between r and β is, therefore

$$\frac{d\beta}{\beta} = -\frac{dr}{r}. \tag{12}$$

The above argument is valid also for the emitter with a small protrusion. If we have a small protrusion on the base emitter, the field is further enhanced by a factor of $m + h/r_p$, where h and r_p are the height and apex radius of the protrusion, m is geometry dependent constant.[46] If we want to analyze more in detail, we should determine both h and r_p. At this stage, it is far too difficult to determine both parameters. Taking this effect into consideration, we can write

$$r = r_a / \left(m + \frac{h}{r_p} \right), \tag{13}$$

where r_a is a radius of the base emitter. From this equation, change in r_p together with that in h is converted to the change in r.

The relation between α and r is now modified to

$$\frac{\delta\alpha}{\alpha} = 2\frac{\delta r}{r} - \frac{0.95bk\phi^{3/2}}{A}\delta r. \tag{14}$$

Integrating Eq. (14), we obtain

$$\alpha = \alpha_0 \left(\frac{r}{r_0} \right)^2 \exp\left(-\frac{0.95bk\phi^{3/2}(r - r_0)}{A} \right)$$

$$= \alpha_0 \left(\frac{r}{r_0} \right)^2 \exp\left(\frac{r - r_0}{r_n} \right), \tag{15}$$

where α_0 and r_0 are integration constants and $r_n = -A/0.95bk\phi^{3/2}$. This relation means that α rapidly increases where $r > r_0$ and the rate of increase is determined by r_n. Assuming $\phi = 5.32$ eV[47] and $k = 1$, we obtain $r_n = 1.04 \times 10^{-9}$ m for the virgin cathode with A of −82.4 V. At present, it is rather difficult to define r_n, r_0, and α_0 in a theoretical way; r_n can be derived from the experimental results. Since r_0 and α_0 are related to each other, once we determine r_0, α_0 is determined automatically.

Here we assume that the difference in A corresponds to the difference in ϕ. That is, r_n is independent of the work function and is a constant. We will argue for the different situation later in Sec. V C. This assumption leads the following formula:

$$-\phi^{3/2}/A = \text{const} = D. \tag{16}$$

We already reported the analysis of ϕ of the Pt cathodes with this assumption in the previous article,[46] and the estimated values are given in Table I. To determine the constant D, ϕ of the virgin cathode should be assumed. In the previous article, we assumed ϕ of the virgin cathode as 5.0 eV, but here we assumed 5.32 eV.[47] This leads $D = 0.149\ \text{eV}^{3/2}\,\text{V}^{-1}$; ϕ is reduced to 3.77 eV after the second treatment, and consequently the reduction in ϕ was 1.5 eV. The reductions in ϕ for the CO-treated cathode agree with the reports that describe the carbon layer formation on the Pt emitter.[48,49]

In the previous article, however, we did not mention B_c. Here we discuss B_c. Taking the following relationship:

$$B_c = M_c - AN_c \tag{17}$$

into consideration, we can calculate $-B_c/A$ in a following manner:

$$-\frac{B_c}{A} = \log_{10}\left(\frac{\alpha_0 a}{1.1\phi k^2 r_0^2} \right) - \frac{1}{\ln 10}\frac{r_0}{r_n} + \frac{1}{\ln 10}\frac{N_n'}{\phi^{1/2}}, \tag{18}$$

which does not depend upon r. It should be noted that the first term on the right-hand side includes kr_0. Although r_0 and α_0 are not known at present, these are integration constants; $\alpha = \alpha_0$ when $r = r_0$. This means that when we determine r_0, then α_0 is determined automatically. Here we define r_0 for simplicity in calculation

$$r_0 = r_n = 1.04 \times 10^{-9}\ \text{m}. \tag{19}$$

The cathode showed $B_c = -757$ V and $-B_c/A = -9.18$ before CO treatment. Assuming $\phi = 5.32$ eV, we can calculate $\alpha_0 = \alpha_n = 3.76 \times 10^{-22}\ \text{m}^2$, which is almost 0.2 by 0.2 Å. Consequently, the formula for the emission area α becomes

$$\alpha = 3.76 \times 10^{-4} r^2 \exp\left(\frac{r}{10.4} - 1 \right), \tag{20}$$

where units for α and r are Å^2 and Å. If we have an emitter with the radius of 10 nm = 100 Å, $\alpha = 2.03 \times 10^4$ Å^2.

The above argument can be summarized as follows. The FN characteristic of the Spindt-type Pt field emission cathode deviates and these FN characteristics go through the following common point:

$$\left(-\frac{1}{A},-\frac{B_c}{A}\right)=\left(\frac{1}{0.95b\phi^{3/2}kr_n},\log_{10}\left[\frac{\alpha_n a}{3.0\phi k^2 r_n^2}\right]+\frac{1}{\ln 10}\frac{N_n'}{\phi^{1/2}}\right), \tag{21}$$

where we replaced the base of natural logarithm with 2.73. Since $-1/A$ does not include the apex radius r, this term is independent of r; $-B_c/A$ does not include r, either. Instead, $kr_n=\beta_n$. This point is determined when ϕ and k are defined. So far, evaluation of the field emission property was made with the slope or both slope and intercept,[50] of one FN plot. Since these values deviate, thus it is difficult to give a certain value as a figure of merit for one cathode. If we use the characteristic point $(-1/A,-B_c/A)$, these values are independent of r, and thus they can be a kind of figures of merit of the field emission cathode.

C. Presence of intersection

The FN characteristics of an identical emitter with different work functions locate along the lines with different slopes. These lines also hold the same point of which coordinates are (P,Q). In the present case, $(P,Q)=(-8.4,-60)$. The lines that go through this (P,Q) in the SK chart are expressed by

$$M_c=A(N_c-P)+Q=AN_c+Q-AP. \tag{22}$$

This means

$$B_c=-AP+Q \tag{23}$$

and $(-1/A,-B_c/A)$ could be written as $(-1/A,P-Q/A)$. From this equation, we can easily obtain the following equation:

$$y=P+Qx. \tag{24}$$

Equation (24) means that the characteristic points for the identical shape but with different work function distribute along a line in the FN diagram. Figure 18 shows the motion of $(-1/A,-B_c/A)$, which is described by Eq. (24) in the FN diagram. Solid circles are experimentally obtained values. In the figure, equi-current lines are shown by solid lines. In the figure, the FN characteristics that have the steepest and gentlest slopes for virgin, first CO-treated, and second CO-treated cathodes are also illustrated by thick solid lines labeled with (0), (1), and (2), respectively. The reason for the difference between the solid circle and the FN characteristics is that the FN characteristics deviate from the fitted line in Fig. 13. Since Q is negative, the line expressed by Eq. (24) has a negative slope.

Since $-B_c/A$ is given by Eq. (21), the following relation should hold:

$$\log_{10}\left(\frac{\alpha_n a}{3.0\phi k^2 r_n^2}\right)+\frac{1}{\ln 10}\frac{N_n'}{\phi^{1/2}}=P-\frac{Q}{A}=P+\frac{QD}{\phi^{3/2}}. \tag{25}$$

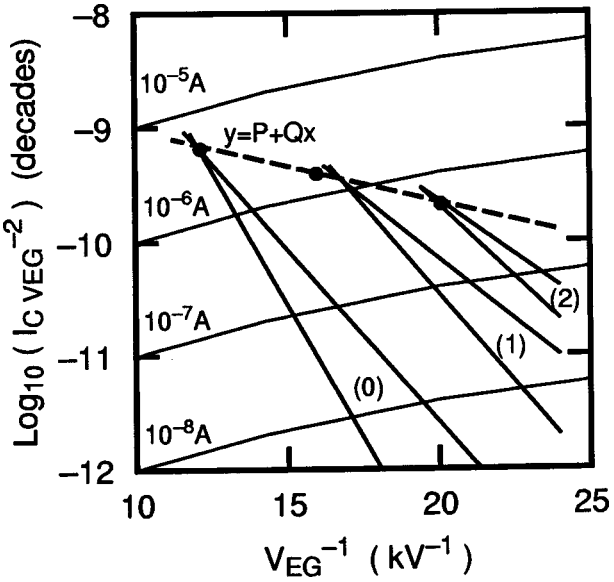

FIG. 18. Motion of the characteristic points of $(-1/A,-B_c/A)$ for the virgin (0), first CO-treated (1), and second CO-treated (2) Pt cathodes in the FN diagram.

The first and the second terms on the left-hand side should correspond to the first and the second terms on the right-hand side, because there is no term which is strongly dependent on ϕ on the left-hand side other than the second term. We still have problems with the different dependence of the second terms on the left- and right-hand sides on ϕ. The term $N_n'/\phi^{1/2}$ is the term due to the image force correction, and it may vary upon the approximation of $v(y)$. If $v(y)$ has y^3 component, the numerator of the image force correction term should have a dependence of $\phi^{3/2}$. We examined the dependence of $v(y)$ on y,[51] but the third order component was sufficiently small as compared to the second order component.

If the argument of this section is valid, the hypothesis we made in the previous section, that is, $-\phi^{3/2}/A=\text{const}$ will become different. To satisfy Eq. (25)

$$-\frac{\phi^{3/2}}{A}\propto\phi, \quad \text{that is,} \quad \phi\propto(-A)^2. \tag{26}$$

If we re-calculate ϕs of CO-treated cathodes with the above equation, they will become 3.07 and 1.94 eV for the first and the second CO-treated cathodes, respectively. It is hard to believe these values, and the argument made in the previous section will be correct rather than that in this section. The values of the second term on the left-hand side and right-hand side of Eq. (25) are 1.85 and 0.728, respectively, and these values, of course, do not coincide. The theoretically drawn value is larger than the experimentally obtained value by a factor of approximately 2. These relationships between the theoretically and experimentally derived values are also similar for the CO-treated cathodes, as shown in Table II.

Here again we would like to argue P. If Q corresponds to the image force correction term, the rest of the pre-exponential term in FN equation, that is, the first term on the left-hand side of Eq. (25), corresponds to the first term on the right-hand side

TABLE II. Comparison of $-Q/A$ and $N_n'/(\phi^{1/2}\ln 10)$.

Parameters Units	Estimated ϕ eV	$X=-Q/A$ (Dimensionless)	$Y=N_n'/(\phi^{1/2}\ln 10)$ (Dimensionless)	Ratio Y/X (Dimensionless)
Virgin	5.32	0.728	1.85	2.54
After 1st CO treatment	4.39	0.958	2.03	2.12
After 2nd CO treatment	3.77	1.20	2.19	1.83

$$\log_{10}\left(\frac{\alpha_n a}{3.0\phi k^2 r_n^2}\right)=P. \tag{27}$$

From this equation, we can again calculate α_n. Since $P=-8.4$, α_n is calculated as $4.36\times10^{-20}\,\mathrm{m}^{-2}$, which is much more likely as compared to α_n derived from Eq. (18).

D. Semiempirical field emission equation

From the above argument, we can describe a semiempirical field emission equation, Unknown Q has a dimension of voltage, thus we write it here as $V_n(=Q\cdot\ln 10)$

$$I=\alpha J=\frac{\alpha_n}{k^2 r_n^2}\exp\left(\frac{r-r_n}{r_n}\right)\frac{aV^2}{\phi}\times\exp\left(-\frac{b\phi^{3/2}kr}{V}\right)\exp\left(\frac{V_n}{b\phi^{3/2}kr_n}\right), \tag{28}$$

where we erased 0.95 and 1.1, because use of 0.95 and 1.1 intead of 1 has now little sense.

If we know the macroscopic field enhancement factor k and work function ϕ, it is possible to write down the equation of the field emission current with the empirically obtained value of V_n. So far, we could only compare the field emission characteristics qualitatively, even in the SK chart. However, if we calculate k, we can draw the grids for the equi-work function lines and equi-apex radius lines, and this will give the ''SK chart'' a role of the ''chart'' in the true sense

$$N_c=\frac{1}{\ln 10}\frac{r-r_n}{r_n}+\log_{10}\left(\frac{\alpha_n a}{\phi k^2 r_n^2}\right)+\frac{1}{\ln 10}\frac{V_n}{b\phi^{3/2}kr_n},$$
$$M_c=\frac{-b\phi^{3/2}kr}{\ln 10}. \tag{29}$$

Substituting the second equation of Eq. (29) into the first equation of Eq. (29), we obtain the equi-apex radius line and the equi-work function line. Figure 19 shows the grids for the present Spindt-type Pt cathode. The solid and the broken lines show the equi-work function line and the equi-apex radius line, respectively. In this figure, the data shown in Fig. 13 are also illustrated. The data distribute along the equi-work function line, as a consequence of our assumption. The equi-apex radius lines stand almost vertically, and they bend towards left at the upper side. It is interesting to see that the experimentally obtained distibution of FN plots in the SK chart also shifted to the left as ϕ decreased, as shown in the figure. The intersections of the different equi-work function lines differ slightly, and this is also similar to the experimental result. If these grids are reliable, it is also said that ϕ of the emitter after exposure to O_2 gas ambient did not recover so much, judging from Figs. 17(a) and 17(b).

One of the problems left is to give the physical basis of the $\phi^{3/2}$ dependence of the image force correction term: what is V_n? And also what does r_n mean? As many researchers pointed out, the FN theory is essentially for a one-dimensional model. The practical emitter is by no means plain, and thus the effect of three-dimensional geometry should be taken into account; for example, α changes with the applied field.[34,44] Another problem is the very strong dependence of the effective α on r. Further investigation will be necessary to establish a complete model of field emission.

VI. CONCLUSION

The electron emission properties of the Spindt-type Pt field emission cathodes in UHV and in gas ambient were investigated in detail. As a result, it was found that even in UHV, the FN characteristics deviated during 150 h operation. These deviating FN characteristics distributed along a straight line in the SK chart. Observation of the emission pattern revealed that our hypothesis on the interpretation of the SK chart is correct: the upper left side indicates the smaller emission area. By operating in CO gas ambient under the appropriate condition, the electron emission property was significantly improved. The effect of the improvement continued for more than 400 h. The improved FN characteristics also distributed along another linear line in the SK

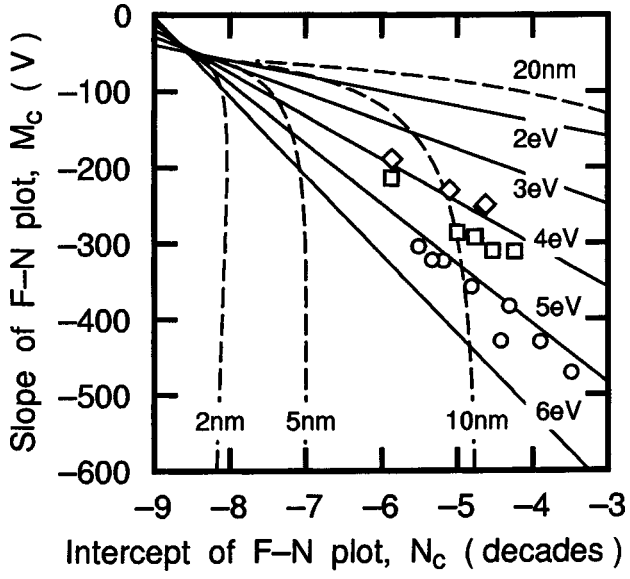

FIG. 19. Grids for the SK chart: equi-work function line is shown by solid line and equi-apex radius line is shown by broken line.

chart. We argued the necessary condition for the linear distribution of FN characteristics, and derived that the emission area should obey the exponential function of the apex radius. We proposed the figures of merit derived from the FN characteristics from an engineering point of view. As a result of the course of the research, we have drawn an empirical formulation of the field emission current as a function of voltage, and gave the grids of equi-work function lines and the qui-apex radius lines for the SK chart.

[1] See, for example, *Proceedings of Asia Display and International Display Workshops*, Nagoya, Japan, 16-19 October, 2001.
[2] R. Mayer, Technical Digest of the Fourth International Vacuum Microelectronics Conference, IVMC'91, Nagahama, Japan, 22-24, August, 1991, p. 6.
[3] H. H. Busta, *Field Emission Flat Panel Displays*, in *Vacuum Microelectronics*, edited by W. Zhu (Wiley, New York, 2001).
[4] C. A. Spindt, I. Brodie, L. Humphrey, and E. R. Westerberg, J. Appl. Phys. **47**, 5248 (1976).
[5] C. A. Spindt, I. Brodie, C. E. Holland, and P. R. Schwoebel, *Spindt Field Emitter Arrays, in Vacuum Microelectronics*, edited by W. Zhu (Wiley, New York, 2001).
[6] G. W. Timm and A. Van der Ziel, Physica (Amsterdam) **32**, 1333 (1966).
[7] Ch. Kleint, Surf. Sci. **25**, 394 (1971).
[8] R. Gomer, Surf. Sci. **38**, 373 (1973).
[9] Ch. Kleint, Surf. Sci. **200**, 472 (1988).
[10] S. Itoh, T. Watanabe, K. Ohtsu, M. Taniguchi, S. Uzawa, and N. Nishimura, J. Vac. Sci. Technol. B **13**, 487 (1995).
[11] P. R. Schwoebel, C. A. Spindt, and I. Brodie, J. Vac. Sci. Technol. B **13**, 338 (1995).
[12] M. Nagao, K. Utsumi, Y. Gotoh, H. Tsuji, J. Ishikawa, T. Nakatani, T. Sakashita, and K. Betsui, Appl. Surf. Sci. **146**, 182 (1999).
[13] W. A. Mackie, T. Xie, and P. R. Davis, J. Vac. Sci. Technol. B **17**, 613 (1999).
[14] C. A. Spindt, C. E. Holland, A. Rosengreen, and I. Brodie, IEEE Trans. Electron Devices **ED38**, 2355 (1991).
[15] S. Itoh, T. Niiyama, and M. Yokoyama, J. Vac. Sci. Technol. B **11**, 647 (1993).
[16] B. R. Chalamala, R. M. Wallace, and B. E. Gnade, J. Vac. Sci. Technol. B **16**, 2855 (1998).
[17] B. R. Chalamala, R. M. Wallace, and B. E. Gnade, J. Vac. Sci. Technol. B **16**, 2859 (1998).
[18] B. R. Chalamala, R. M. Wallace, and B. E. Gnade, J. Vac. Sci. Technol. B **16**, 2866 (1998).
[19] B. R. Chalamala, R. M. Wallace, and B. E. Gnade, J. Vac. Sci. Technol. B **16**, 3073 (1998).
[20] B. R. Chalamala, R. M. Wallace, and B. E. Gnade, J. Vac. Sci. Technol. B **17**, 303 (1999).
[21] Y. Gotoh, K. Utsumi, M. Nagao, H. Tsuji, J. Ishikawa, T. Nakatani, T. Sakashita, and K. Betsui, J. Vac. Sci. Technol. B **17**, 604 (1999).
[22] Y. Gotoh, D. Nozaki, H. Tsuji, J. Ishikawa, T. Nakatani, T. Sakashita, and K. Betsui, Appl. Phys. Lett. **77**, 588 (2000).
[23] Y. Gotoh, D. Nozaki, H. Tsuji, J. Ishikawa, T. Nakatani, T. Sakashita, and K. Betsui, J. Vac. Sci. Technol. B **19**, 912 (2001).
[24] R. Gomer, *Field Emission and Field Ionization* (Harvard University Press, Cambridge, 1961).
[25] F. M. Charbonnier and E. E. Martin, J. Appl. Phys. **33**, 1897 (1962).
[26] Y. Gotoh, M. Nagao, M. Matsubara, K. Inoue, H. Tsuji, and J. Ishikawa, Jpn. J. Appl. Phys., Part 2 **35**, L1297 (1996).
[27] T. Nakatani, T. Sakashita, O. Toyoda, K. Inoue, T. Kosaka, N. Kondo, S. Fukuta, and K. Betsui, *Proceedings of the Third International Display Workshops, IDW'96*, Kobe, Japan, 27-29 November 1996, p. 127.
[28] D. Nicolaescu, J. Vac. Sci. Technol. B **13**, 531 (1995).
[29] J. Ishikawa, H. Tsuji, Y. Gotoh, T. Sasaki, T. Kaneko, M. Nagao, and K. Inoue, J. Vac. Sci. Technol. B **13**, 308 (1993).
[30] M. Nagao, Y. Fujimori, Y. Gotoh, H. Tsuji, and J. Ishikawa, J. Vac. Sci. Technol. B **16**, 829 (1998).
[31] M. Nagao, Y. Gotoh, T. Ura, H. Tsuji, and J. Ishikawa, J. Vac. Sci. Technol. B **17**, 623 (1999).
[32] Y. Gotoh, H. Tsuji, and J. Ishikawa, *Extended Abstracts of the Third International Vacuum Electron Sources Conference, IVESC2000*, Orlando, FL, 10–13 July, 2000 (IEEE, New York, 2000), p. B-5.
[33] M. Nagao, T. Kondo, Y. Gotoh, H. Tsuji, J. Ishikawa, K. Miyata, and K. Kobashi, Appl. Phys. Lett. **71**, 2806 (1997).
[34] J. Ishikawa, H. Tsuji, K. Inoue, M. Nagao, T. Sasaki, T. Kaneko, and Y. Gotoh, Jpn. J. Appl. Phys., Part 2 **32**, L342 (1993).
[35] M. Nagao, M. Matsubara, K. Inoue, Y. Gotoh, H. Tsuji, and J. Ishikawa, Jpn. J. Appl. Phys., Part 1 **35**, 5479 (1996).
[36] M. Watanabe, K. Tanaka, O. Nishikawa, T. Yamaguchi, N. Choi, and H. Tokumoto, in Ref. 32, p. F-3.
[37] W. A. Mackie, T. Xie, and P. R. Davis, Technical Digest of the 15th International Vacuum Microelectronics Conference and the 48th International Field Emission Symposium, IVMC/IFES2002, Lyon, 7–11 July, 2002 (2002), OB1.01.
[38] K. Utsumi, M. Nagao, Y. Gotoh, H. Tsuji, J. Ishikawa, T. Nakatani, T. Sakashita, K. Inoue, and K. Betsui (unpublished).
[39] Y. Gotoh, H. Tsuji, and J. Ishikawa, J. Vac. Sci. Technol. B **19**, 992 (2001).
[40] V. T. Binh and S. T. Purcell, Appl. Surf. Sci. **111**, 157 (1997).
[41] K. Nakamura, H. Nakahara, Y. Gotoh, H. Tsuji, and J. Ishikawa, Extended Abstracts of 50th Spring Meeting of The Japan Society of Applied Physics and Related Societies, 29p-YL-12/II, 28-31 March, 2003, p. 817 (in Japanese).
[42] R. H. Good, Jr. and E. W. Müller, in *Handbuch der Physik*, edited by S. Flügge (Springer, Berlin, 1956), p. 176.
[43] R. G. Forbes, J. Vac. Sci. Technol. B **17**, 526 (1999).
[44] R. G. Forbes and K. L. Jensen, Ultramicroscopy **89**, 17 (2001).
[45] Y. Gotoh, H. Tsuji, and J. Ishikawa, Ultramicroscopy **89**, 63 (2001).
[46] R. G. Forbes, C. J. Edgcombe, and U. Valdrè, Ultramicroscopy **95**, 57 (2003).
[47] V. S. Fomenko, *Handbook of Electron Emission Property*, translated by Nisso Tsushinsha (Nisso Tsushinsha, Wakayama, 1973) [in Japanese].
[48] X. Q. D. Li, T. Radojicic, and R. Vanselow, Surf. Sci. **225**, L29 (1990).
[49] I. D. Hughes and H. M. Montagu-Pollack, J. Phys. D **3**, 228 (1970).
[50] J. Kai, M. Kanai, M. Tama, K. Ijima, and K. Tawa, Jpn. J. Appl. Phys., Part 1 **40**, 4696 (2001).
[51] R. E. Burgess, H. Kromer, and J. M. Houston, Phys. Rev. **90**, 515 (1953).